Taylor & Francis
Taylor & Francis Group

Supramolecular interactions in a family of dinuclear helicates in the solid-state

Benjamin H. Wilson & Paul E. Kruger

Taylor & Francis
Taylor & Francis Group

ARTICLE

Check for updates

Supramolecular interactions in a family of dinuclear helicates in the solid-state

Benjamin H. Wilson [ID]a,b and Paul E. Kruger [ID]a

aMacDiarmid Institute for Advanced Materials and Nanotechnology, School of Physical and Chemical Sciences, University of Canterbury, Christchurch, New Zealand; bDepartment of Chemistry and Biochemistry, University of Windsor, Windsor, Ontario, Canada

ABSTRACT

Metallo-helicates are a commonly encountered assembly within supramolecular chemistry. Interest in these architectures stems from their inherent helical chirality which positions them for a diverse range of applications such as catalysis and non-linear optics (NLO). The current study uses Co(II) dinuclear double helices as versatile supramolecular synthons. The ditopic ligand, **L**, features two tridentate quinolinyl-hydrazone binding sites imparting it with hydrogen bond donors and π-faces for secondary supramolecular interactions. Incorporation of **L** into $[Co_2(\mathbf{L})_2]^{4+}$ helical assemblies results in a helical cationic supramolecular synthon with moieties predisposed to forming π-π stacking and hydrogen bond interactions. The single-crystal X-ray structures of $[Co_2(\mathbf{L})_2]X_4$ (X = ClO_4^-, BF_4^- and $CF_3SO_3^-$) revealed a variety of anion dependent hydrogen bond networks arising through the interaction of the hydrazide hydrogen with the anion. These interactions in turn strongly influence the nature of the π-π stacking interactions of the quinoline moieties which can be analysed via the Hirshfield surface.
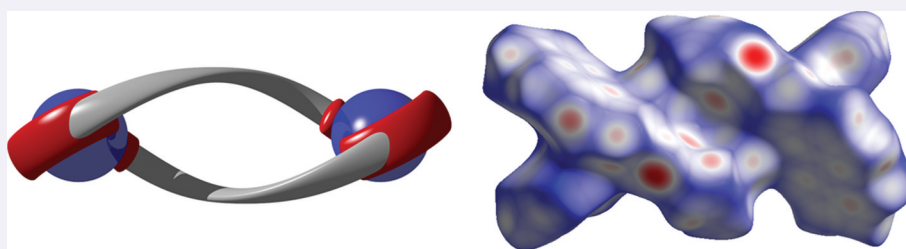
Introduction

Metallo-helicates are a widely studied form of metallo-supramolecular assembly [1–3]. The combination of metal centres and organic ligands has resulted in many double, triple and quadruple stranded helicates that possess a diverse range of properties such as redox activity [4–7], fluorescence [8–11], spin crossover [12–22] and single-molecule magnetism [9,23–25]. Furthermore, topologically complex circular helicates can be utilised as building blocks for the synthesis of mechanically intertwined molecular knot assemblies [26–28]. Much of the interest in helicate structures stems from the intrinsic chirality adopted by the twisted conformation of the bridging ligands [29]. The helical chirality of these supramolecular assemblies makes them highly suictable candidates for DNA binding [10,30–32] or asymmetric catalysis [33]. Optimisation of the interaction of metallo-helicates with chiral substrates requires a thorough understanding of

their supramolecular interactions. It is this avenue of research that has led to metallo-helicates becoming prominent assemblies in crystal engineering and their use as supramolecular synthons [34,35]. The ligands provide a point of attachment functionality capable of forming supramolecular interactions with neighbouring molecules or counter anions. These functionalities may orient into specific directions relative to one another upon coordination of the ligands to the metal ions to form the helical structure, resulting in a highly directionally specific supramolecular synthon. Our group is concerned with the synthesis of dinuclear M(II) helicates and mesocates [12–14,36,37]. Recently our attention has been focused on the use of ligands incorporating the pyrazinyl-hydrazone coordinating moiety. This work highlighted the applicability of such dinuclear supramolecular assemblies as supramolecular synthons via the ability of the hydrazide (N)H to act as a potent hydrogen bond donor [37]. Flexible

ligands derived from a succinic acid core featuring pyridyl-hydrazone coordinating groups have been recently reported to form dinuclear double helices upon complexation with Co(II) and displayed single-molecule magnetism and catalytic behaviour [25,33]. Herein we report the synthesis of a related novel ligand, **L**, featuring the quinolinyl-hydrazone coordinating moiety (Figure 1). The introduction of a larger quinoline aromatic functionality should introduce a greater tendency for π-π stacking [38]. In conjunction with the potent hydrazide hydrogen bond donor [39–42,43], the incorporation of this ligand into a Co(II) dinuclear double helicate results in a versatile cationic supramolecular synthon. This work investigates the variation of the crystal packing of these helices upon modulation of the counter anion and seeks to rationalise the importance of hydrogen bonding and π-π interactions on the resultant structures. Analysis of the Hirshfeld surfaces provided further insight into the importance of the supramolecular interactions occurring between complexes in each of their crystal lattices.

Materials and methods

All reagents and solvents used were of reagent grade unless otherwise stated and did not require further purification. In-house distilled water was used. Chemicals were sourced from Sigma Aldrich and used as received. All reactions were carried out in air unless otherwise stated. ^{1}H and ^{13}C NMR measurements were carried out on an Agilent 400 MR spectrometer operating at 400 MHz for ^{1}H and 101 MHz for ^{13}C. Chemical shift values are given in parts per million (PPM). Melting points were carried out on an Electrothermal melting point apparatus and are uncorrected. FT-IR spectra for organic compounds were recorded a Bruker ALPHA Platinum ATR FT-IR spectrometer measuring in the range 4000–450 cm^{-1}. The following abbreviations were used to describe the signals: s (strong), m (medium), w (weak), br (broad). Mass spectrometry experiments were carried out on a Bruker maXis 4 G time of flight spectrometer operating in ESMS+ mode. Values are given as MH+ (unless otherwise stated). TGA measurements were performed on an Alphatech SDT Q600 TGA/DSC under an inert nitrogen atmosphere. Samples were

heated from 10°C to 800°C at a rate of 1.5°C min^{-1}. For C, H, N analysis, samples were sent to Campbell Microanalytical Laboratories, Otago University, Dunedin. Samples were dried to constant weigh before analysis. *Caution is advised when handling perchlorate salts as they are potentially explosive.*

Ligand synthesis

Succinyl hydrazide
Succinyl hydrazide was synthesised following a literature preparation [44]. Diethyl succinate (2.8 mL, 17 mmol) and hydrazine monohydrate (4.2 mL, 85 mmol) were added sequentially to ethanol (10 mL) and the solution was heated at reflux for 12 hours during which a white crystalline precipitate formed. After cooling to room temperature, the white precipitate was filtered and washed with ethanol then diethyl ether (1.25 g, 11 mmol, 65% yield). M.pt. 158°C–160°C Lit. 166°C, δ_H (400 MHz, [d$_6$]-DMSO): 8.95 (s, 1 H, H$_{NH}$), 4.12 (s, 2 H, H$_{NH}$), 2.23 (2 H, s, H$_{alkyl}$), ESI-MS: meas. 147.0877 ([M + H]$^+$), [C$_4$H$_{11}$N$_4$O$_2$]$^+$ calc. 147.0877

(N'1E,N'4E)-N'1,N'4-bis(quinolin-2-ylmethylene)succinohydrazide, L
Quinoline-2-carbaldehyde 1.6 g, 10 mmol was dissolved in ethanol (50 mL) at reflux. Succinic dihydrazide (0.5 g, 4.4 mmol) was added to give a brown suspension which was heated at reflux overnight. The brown suspension was then cooled to room temperature and filtered then washed with boiling ethanol and oven dried for one hour at 70 °C to give a pale brown solid (1.1 g, 2.6 mmol, 60% yield). M.pt. 255°C–260°C (decomposition), δ_H (400 MHz, [d$_6$]-DMSO) 11.70 (s, 1 H, H$_{NH}$), 8.36 (m, 2 H, H$_{quinoline}$), 8.18 (1 H, s, H$_{imine}$), 8.02 (m, 2 H, H$_{quinoline}$), 7.77 (t, J = 7.6, 1 H, H$_{quinoline}$), 7.62 (m, 1 H, H$_{quinoline}$), 3.08 (s, 2 H, H$_{alkyl}$), Low solubility precluded analysis by ^{13}C NMR, ESI-MS: meas. 213.0896 ([M + 2 H]$^{2+}$), [C$_{24}$H$_{22}$N$_6$O$_2$]$^{2+}$ calc. 213.0897, IR: (v_{max}/cm^{-1}) 3062 (w), 2988 (w), 2950 (w), 2899 (w), 1669 (s) 1639 (w), 1588 (m), 1558 (w), 1519 (w), 1504 (m), 1458 (m), 1441 (m), 1429 (w), 1397 (s), 1349 (w), 1327 (w), 1311 (m), 1300 (m), 1237 (w), 1205 (m) 1153 (s), 1142 (s), 1113 (m), 1018 (w), 995 (w), 977 (m), 942 (s), 902 (m), 881 (w), 839 (s), 806 (s), 790 (m), 774 (m), 755 (s), 692 (w), 644 (w), 621 (m)
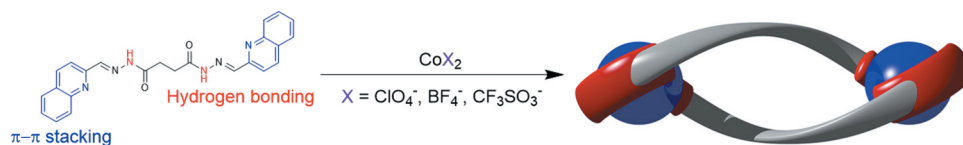
Figure 1. (colour online) The ligand, **L**, reported in this work featuring the hydrazone and quinoline moieties. The combination of **L** with CoX$_2$ (X$^-$ = ClO$_4^-$, BF$_4^-$ and CF$_3$SO$_3^-$) results in the formation of a dinuclear double-stranded helicate of the generalised formula [Co$_2$(**L**)$_2$]X$_4$, represented schematically.

Complex synthesis

[Co$_2$(L)$_2$](ClO$_4$)$_4$, 1

Co(ClO$_4$)$_2$ · 6H$_2$O (8.6 mg, 23.6 μmol) was dissolved in acetonitrile (15 mL) and was stirred at room temperature. **L** (10 mg, 23.6 μmol) was added to give a pale brown/yellow suspension and stirred for approximately 5 hours to give an orange/brown cloudy solution. The cloudy solution was allowed to stand at room temperature for 2 hours and then filtered to give a yellow/brown solution. Vapour diffusion of benzene into the filtrate resulted in orange block crystals suitable for single crystal X-ray diffraction. Found: C, 40.53 H, 2.83, N, 11.52% [Co$_2$(C$_{24}$H$_{20}$N$_6$O$_2$)$_2$](ClO$_4$)$_4$ · 5(H$_2$O)·0.25(CH$_3$CN)·0.25(C$_6$H$_6$) requires: C, 40.46 H, 3.55 N, 11.56%, IR: (v_{max}/cm^{-1}) 3527 (w, br.) 290 (w, br.) 1617 (m) 1590 (w) 1554 (m) 1509 (m) 1435 (w) 1404 (w) 1381 (w) 1336 (M) 1299 (w) 1250 (w) 1213 (m) 1176 (m) 1062 (s, br.) 1000 (s) 931 (m) 871 (w) 832 (m) 786 (m) 755 (m) 621 (s)

[Co$_2$(L)$_2$](BF$_4$)$_4$, 2

Co(BF$_4$)$_2$ · 6H$_2$O (8.6 mg, 23.6 μmol) was dissolved in acetonitrile (15 mL) and was stirred at room temperature. **L** (10 mg, 23.6 μmol) was added to give a pale brown/yellow suspension and stirred for approximately 5 hours to give an orange/brown cloudy solution. The cloudy solution was allowed to stand at room temperature for 2 hours and then filtered to give a yellow/brown solution. Vapour diffusion of diisopropyl ether into the filtrate resulted in orange block crystals suitable for single crystal X-ray diffraction. Found: C, 42.37 H, 3.36, N, 12.05% [Co$_2$(C$_{20}$H$_{24}$N$_6$O$_2$)$_2$](BF$_4$)$_4$ · 2.7(H$_2$O) requires: C, 42.31 H, 3.36 N, 12.36%, IR: (v_{max}/cm^{-1}) 3579 (br., w), 3215 (br., w) 3048 (br., w), 1616 (m), 1592 (w), 1545 (m), 1509 (s), 1436 (w), 1405 (w), 1381 (m), 1337 (w), 1299 (w), 1250 (m), 1214 (w), 1177 (w), 1144 (m), 1128 (m), 1017 (s), 992 (s), 936 (m), 872 (w), 835 (m), 786 (m), 750 (m), 699 (w), 679 (w), 617 (w), 593 (w), 569 (w), 519 (m), 486 (m)

[Co$_2$(L)$_2$](OTf)$_4$, 3

CoCl$_2$ · 6H$_2$O (3.6 mg, 23.6 μmol) was dissolved in acetonitrile (5 mL). AgOTf (12.1 mg, 47.2 μmol) was added resulting in the immediate formation of a white precipitate. The solution was filtered into a suspension of **L** (10 mg, 23.6 μmol) in acetonitrile (5 mL). The pale brown/yellow suspension and stirred for approximately 5 hours to give an orange/brown cloudy solution. The cloudy solution was allowed to stand at room temperature for 2 hours and then filtered to give a yellow/brown solution. Vapour diffusion of m-xylene into the filtrate resulted in orange block crystals suitable for single crystal X-ray diffraction. Found: C, 38.24 H, 2.84, N, 10.39% [Co$_2$(C$_{24}$H$_{20}$N$_6$O$_2$)$_2$](CF$_3$SO$_3$)$_4$ · 3.75(H$_2$O) requires: C, 38.30 H, 2.94 N, 10.31%, IR: (v_{max}/cm^{-1}) 3491 (br., w), 3197 (br., w), 2939 (br.,w), 1619 (m), 1589 (w), 1544 (m), 1510 (m), 1436 (w), 1407 (w), 1382 (m), 1336 (w), 1244 (s), 1224 (s), 1166 (s), 1140 (s), 1025 (s), 999 (m), 937 (m), 918 (w), 871 (w), 829 (m), 786 (m), 753 (m), 698 (w), 634 (s), 573 (m), 514 (m), 483 (m)

Results and discussion

The ligand, **L**, was synthesised following adapted literature procedures for analogous ligands [23]. The complexes **1** to **3** were synthesised by complexing the ligand, **L**, with the appropriate CoX$_2$ salt (X = ClO$_4^-$ **1**, BF$_4^-$ **2** and CF$_3$SO$_3^-$ **3**) in acetonitrile. In all cases, a pale yellow/orange solution was obtained, which upon vapour diffusion of an appropriate anti-solvent resulted in orange block crystals suitable for structural analysis via single-crystal X-ray diffraction. All complexes were susceptible to desolvation upon removal from the mother liquor, highlighted by the TGA for **2** and **3** (TGA for **1** was not performed as it contains perchlorate anions). Furthermore, the elemental analysis revealed a tendency for the complexes to undergo hydration under ambient conditions prior to measurement. Complex **1** was synthesised via vapour diffusion of benzene into an acetonitrile solution and crystallised in the monoclinic space group $P2_1/n$. The asymmetric unit is comprised of two Co(II) centres bridged by two **L** ligands coordinating in the expected tridentate fashion (Figure 1, Figure 2 and S3).

Analysis of the C = O bond lengths confirms that the ligand is coordinating in the neutral keto form (table S2). The relevant Co-N/O bond lengths and angles are summarised in tables S3 and S4. The two high spin Co(II) centres exist in a significantly distorted N$_4$O$_2$ octahedral coordination sphere with octahedral distortion parameters (Σ) of 152.8° and 143.3° for Co1 and Co2, respectively [44]. The succinate backbones of the two ligands are significantly twisted, resulting in the ligands adopting a helical conformation about the two Co(II) centres. The geometric parameters for **1** are summarised in table S5. The dinuclear double helicate in the asymmetric unit exhibits P helical chirality while the M enantiomer is generated via the action of the inversion centre present in the centrosymmetric space group. The charge of the [Co$_2$(**L**)$_2$]$^{4+}$ cation is balanced by four perchlorate anions, three of which are modelled as disordered over two positions. We have previously reported the hydrazide (N)H of a related pyrazinyl-hydrazone-based ligand to be a potent hydrogen bond donor [37]. Three of the hydrazide moieties of **1** participate in hydrogen bonding interactions with the perchlorate anions while the fourth participates in a hydrogen bonding interaction with a water molecule, with (N)H⋯O distances ranging from
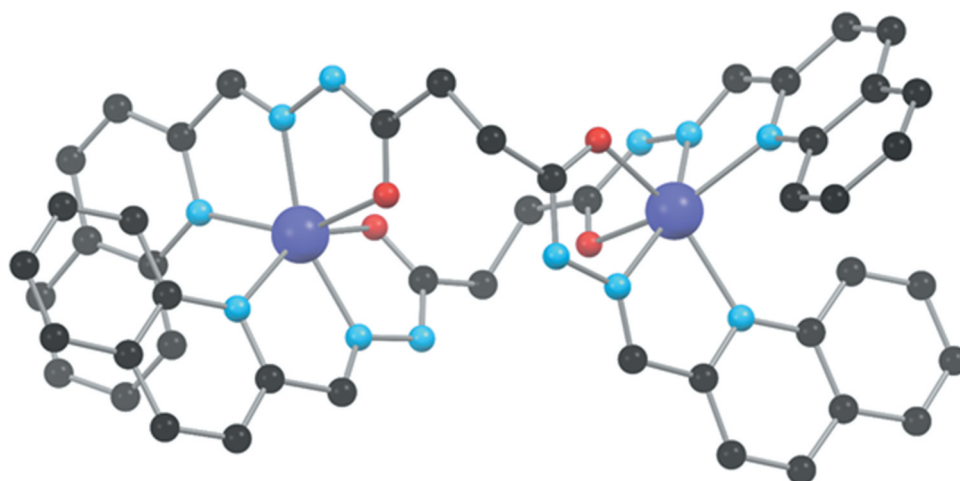
Figure 2. (colour online) Single crystal X-ray structure of **1**, representative for this group of helicate complexes. Two ligands, **L**, coordinate to the Co(II) centres in a tridentate manner via the quinolinyl and hydrazone nitrogen atoms and the hydrazone oxygen atom. Hydrogen atoms, anions and solvent molecules omitted for clarity.

1.905(6) to 2.15(1) Å (figure S6, table S6). The hydrogen atoms of the water molecule also participate in further hydrogen bonding interactions with perchlorate anions, resulting in the propagation of a hydrogen-bonding network. This hydrogen-bonding network forms supramolecular two-dimensional sheets in the crystallographic *ab*-plane. The propensity of the quinoline moieties to form intramolecular [45] and intermolecular [46–48] π-stacked assemblies in metal hydrazone complexes is established in the literature, the latter of which is exemplified by **1**. Two forms of π-π stacking occur at either end of each ligand strand of the helicate (Table S9). At one end of a ligand strand, only the benzo rings of the quinoline moiety over-lap with a π(centroid)···π(centroid) separation of 3.509(4) Å. At the other end, the two pyridyl and benzo rings of the quinoline moieties on neighbouring complexes overlap with π(centroid)···π (centroid) separations of 3.604(4) and 3.666(4) Å, respectively (Figure 3). The propagation of these π-π stacking interactions results in the formation of a supramolecular two-dimensional sheet in the *ac*-crystallographic plane. Complex **1** crystallised with a number of benzene and acetonitrile solvent molecules in addition to one water molecule, many of which are disordered and with partial occupancy. However, only the water molecule participates in the interactions outlined above, responsible for the observed crystal packing.

Complex **2** was synthesised via vapour diffusion of diisopropyl ether into an acetonitrile solution and crystallised in the triclinic space group *P*-1. The composition of the asymmetric unit is broadly similar to **1** and contains an isostructural dinuclear double helicate and therefore, only a brief discussion of salient difference and similarities will be given. The Co(II)-N/O bond lengths and angles are similar to **1** and are summarised in tables S3 and S4. The high spin Co(II) centres exist in N_2O_4 distorted octahedral coordination spheres with Σ parameters of 139.9° and 136.3° for Co1 and Co2, respectively. Likewise, the succinate backbone of the two ligands is significantly twisted as detailed in table S5. Three of the hydrazide (N)H moieties participate in hydrogen bond interactions with tetrafluoroborate anions while the fourth participates in a hydrogen bond interaction with an acetonitrile molecule, with (N)H···A (A = N, O) separations ranging from 1.871(2) to 2.277(5) Å (figure S7, table S7). In contrast to **1**, the tetrafluoroborate anions do not form bridging hydrogen bond interactions between neighbouring complexes, resulting in the absence of a hydrogen bond network. Therefore, while the anions of **1** and **2** have the same geometry, the crystal packing is significantly different. The predominant intermolecular interactions between neighbouring complexes are via π-stacking and edge-to-face (C)H···π interactions of the quinoline moieties. The (C)H moiety in the 6-position of the quinoline ring forms a (C)H···π interaction with the benzene ring of a neighbouring quinoline moiety and *vice versa* in reciprocal fashion. Two crystallographically unique pairs of this interaction occur with H···π(centroid) separations ranging from 2.613(1) to 3.333(3) Å (Figures 3, S9 and table S10). A π-stacking interaction occurs in a manner similar to that observed in **1** where the two pyridine and benzene rings of the quinoline moiety overlap to form a reciprocal interaction. Two crystallographically unique types of this interaction occur with π(centroid)···π(centroid) separations of 3.856(2) and 3.744(2) Å (Figure 4). The combination of the π-stacking and edge-to-face (C)H···π interactions results in the formation of a two-dimensional supramolecular sheet, similar to **1**, however, with a pronounced
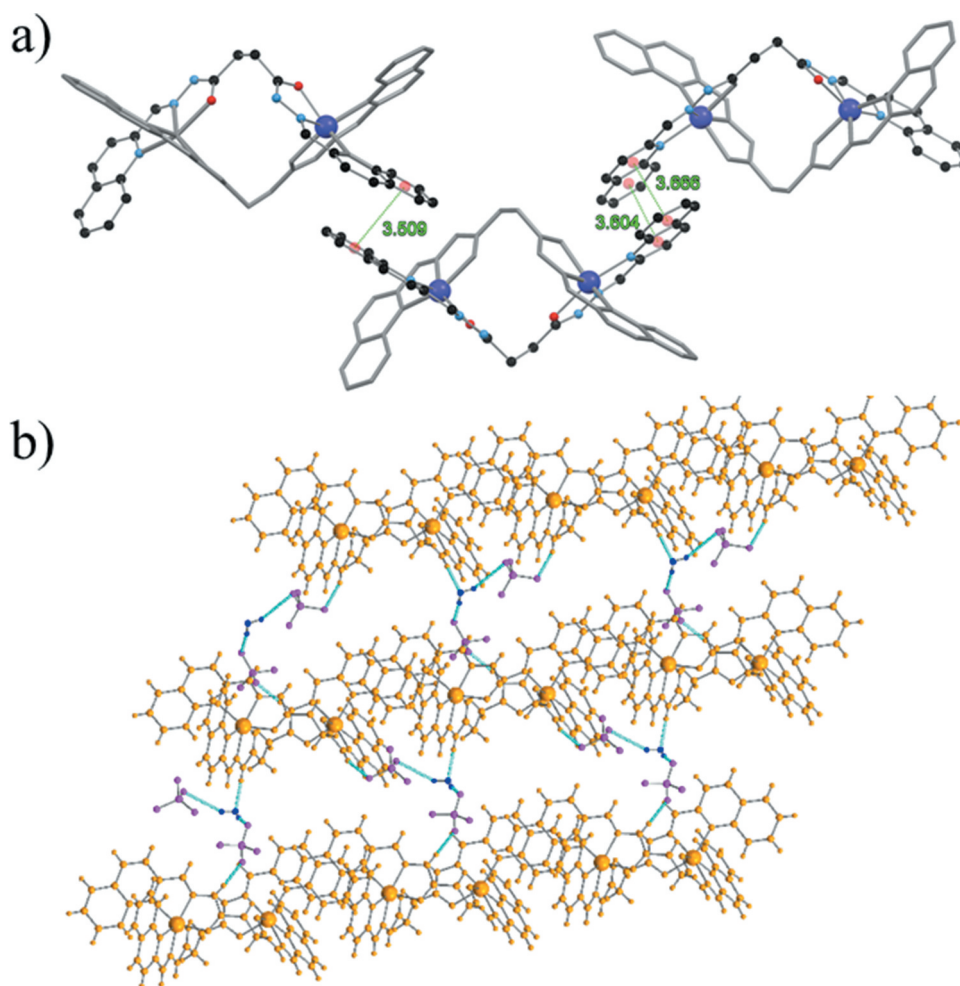
Figure 3. (colour online) (a) The two forms of π-π interactions occurring between the quinoline moieties on neighbouring dinuclear helicates for **1**. The π(centroid) are shown as red spheres while the π(centroid)···π(centroid) separations are shown in green and given in Å. Hydrogen atoms, triflate anions and solvent molecules omitted for clarity. (b) The hydrogen-bonding network of **1** that results in the propagation of a two-dimensional supramolecular sheet. The dinuclear helicates are shown in orange, the perchlorate anions in purple and the water molecules in dark blue. The (N)H···O separations are shown in light blue. Perchlorate anions and solvent molecules not participating in the illustrated interaction are omitted for clarity.

undulating nature. Much like **1, 2** crystallises with a number of solvent molecules in the lattice. There are two disordered acetonitrile solvent molecules and a water molecule. However, only one acetonitrile molecule participates in the hydrogen bond interactions outlined above. The presence of acetonitrile and water molecules is supported by TGA (figure S1). A 7.7% mass loss between 45°C and 113°C can be attributed to complete desolvation of **2** · 2.8(MeCN)·0.2(H$_2$O) to give **2** (8.2%), while the thermal decomposition of **2** occurs above 230°C.

Complex **3** was synthesised via vapour diffusion of *m*-xylene into an acetonitrile solution and crystallised in the triclinic space group *P*-1. The composition of the asymmetric unit is broadly similar to **1** and **2** and contains an isostructural dinuclear double helicate. Therefore, only a brief discussion of similarities and differences to the preceding complexes follows. The Co(II)-N/O bond lengths and angles are broadly similar to **1** and **2** and are summarised in tables S3 and S4. The high spin Co(II) centres exist in N$_2$O$_4$ distorted octahedral coordination spheres with Σ parameters of 140.0° and 132.0° for Co1 and Co2, respectively. Likewise, the succinate backbone of the two **L** ligands is significantly twisted as detailed in table S5. The charge balance is provided by four triflate anions, three of which are disordered. Three of the hydrazide moieties of **3** participate in hydrogen bond interactions with the triflate anions while the fourth participates in a hydrogen bond interaction to a water molecule, with (N)H···O distances ranging from 1.79(2) to 2.221(5) Å (figure S8, table S8). The water molecule acts as a further hydrogen bond donor to two symmetry generated triflate anions resulting in the propagation of a hydrogen-bonding network in
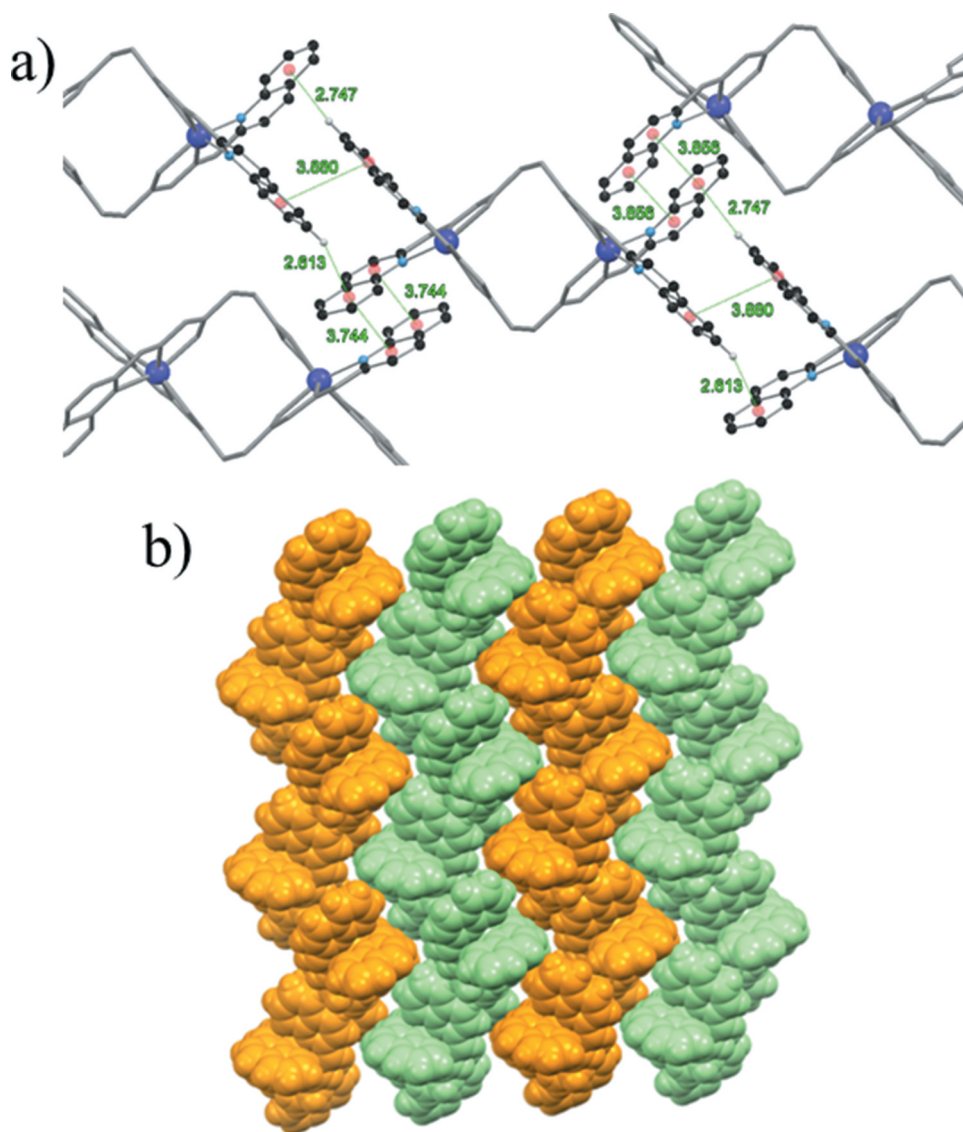
Figure 4. (colour online) (a) π-π and edge-to-face (C)H⋯π interactions occurring for **2** resulting in the propagation of a supramolecular two-dimensional sheet with distances given in Å. The π(centroid) are shown as red spheres while the π(centroid)⋯π(centroid) and H⋯π (centroid) separations are shown in green. Hydrogen atoms, triflate anions and solvent molecules not participating in the illustrated interactions omitted for clarity. (b) The interdigitation of the undulating two-dimensional sheets for **2**, shown alternating in orange and green for clarity.

a similar fashion to **1**. This results in the formation of a hydrogen-bonding chain running approximately parallel to the crystallographic *c*-axis (Figure 5). In a similar fashion to **2**, the quinoline moieties of **3** participate in both π-π stacking and edge-to-face (C)H⋯π interactions (figure S10, Table S11). Two forms of π-staking interactions between neighbouring complexes are present. The first occurs with a π(centroid)⋯π(centroid) separation of 3.556(3) Å. The second occurs with a π(centroid)⋯π(centroid) separation of 3.836(3) Å in conjunction with an edge-to-face C-H⋯π interaction. The combination of these two π-stacking interactions results in the formation of a two-dimensional supramolecular sheet. Complex **3** crystallises with a number of water and

acetonitrile molecules in the lattice, however, only one water molecule participates in the interactions outlined above, responsible for the observed crystal packing. This solvent content is supported by TGA analysis (figure S2). A gradual mass loss of 21.1% occurs between 73°C and 173°C followed by a more rapid mass loss of 3.8% between 207°C and 258°C. It is postulated that upon the removal of the crystals from the mother liquor, 1.5 acetonitrile molecules are lost to give **3** · 1.5(MeCN)·2(H$_2$O). The loss of two water molecules constitutes a mass loss of 2.1% to give **3** · 1.5(MeCN), followed by the loss of 1.5 acetonitrile molecules which constitutes a mass loss of 3.7% to give fully desolvated **3**. A rapid mass loss occurs after 360°C due to complex decomposition.
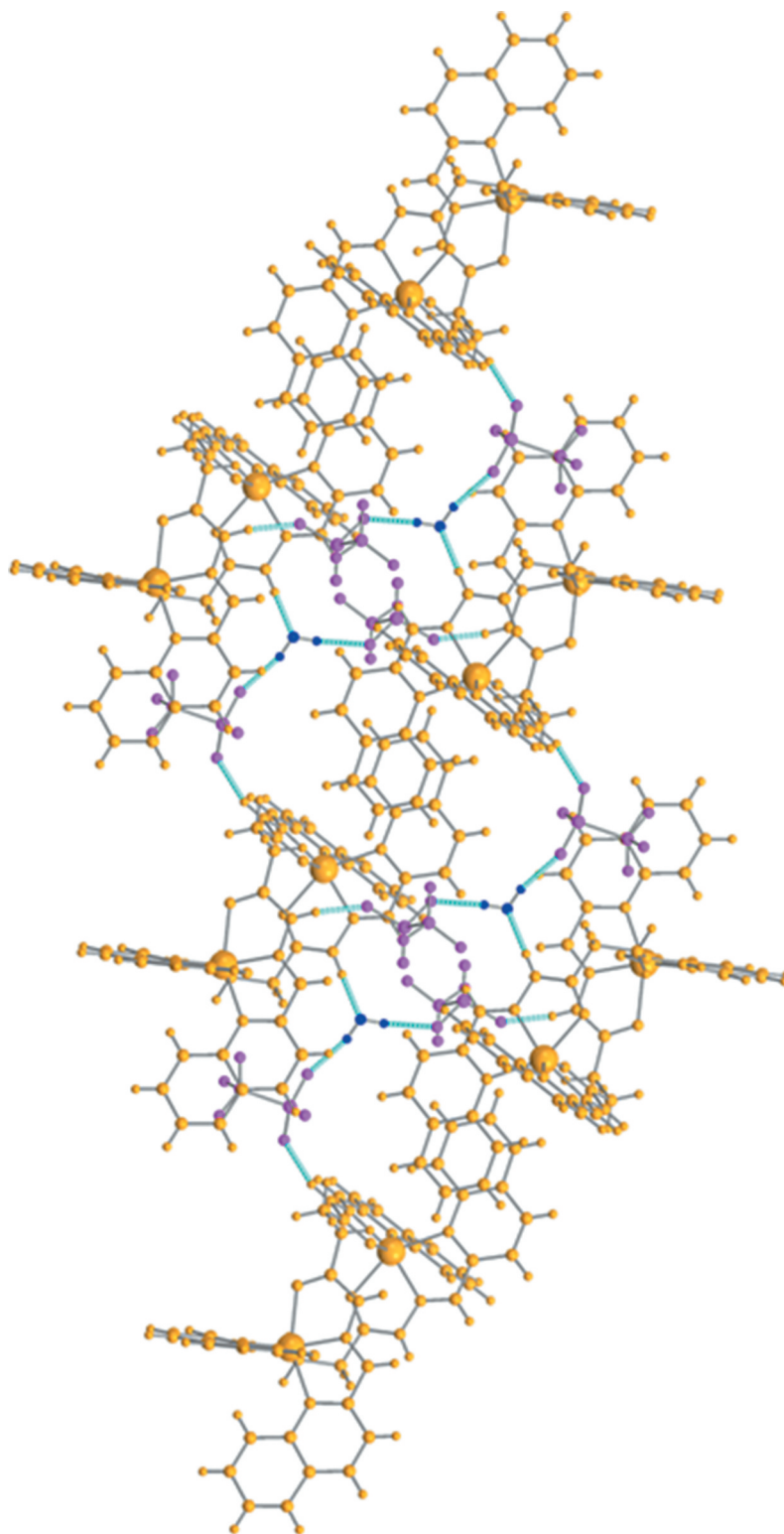
Figure 5. (colour online) The hydrogen-bonding network of **3** resulting in the propagation of a one-dimensional supramolecular chain. The dinuclear helicate units are shown in orange, the triflate anions in purple and the water molecules in dark blue. The (N)H···O and (O)H···O separations are shown in light blue. Triflate anions and solvent molecules not participating in the illustrated interactions are omitted for clarity.

To compare the intermolecular interactions of the complexes in a more quantitative manner, the Hirshfield surfaces [49–51] for **1, 2** and **3** were calculated using Crystal Explorer [52]. Mapping the d_{norm} (normalised contact distance) onto the Hirshfield surface reveals the commonality in the hydrogen bonding of the hydrazide moiety of all three complexes (Figures 6 and S11). Contacts with external molecules shorter than the sum of the Van de Waals radius
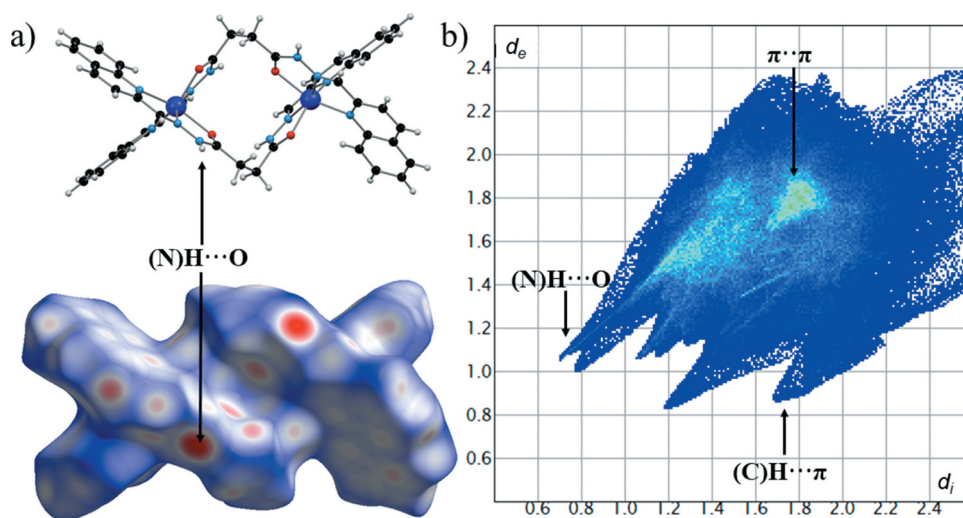
Figure 6. (colour online) (a) The single-crystal x-ray structure and d_{norm} mapped onto the Hirshfield surface of the dinuclear helicate $[Co_2(\mathbf{L})_2]^{4+}$ in **1**. The red region of the Hirshfield surface (d_{norm} shorter than sum of Van de Waals radii) corresponds to the (N)H hydrogen bond donor moiety. (b) The 2D fingerprint plot of **1** highlighting the regions corresponding to the three intermolecular interactions of interest: (N)H···O hydrogen bonding, (C)H···π and π···π interactions. High frequency of d_e and d_i separation is shown in pale green while low frequency dark blue. Hirshfield surface and 2D fingerprint plot were generated using Crystal Explorer [52].

are represented as red areas on the surface in the case of complex **1, 2** and **3** occur around the (N)H moiety of the hydrazide which act as a hydrogen bond donor. Contacts with external molecules greater than the sum of the Van de Waals radius are shown in blue. The normalised contact distance is defined by two parameters: d_e (the distance from the surface to the nearest external nucleus) and d_i (the distance from the surface to the nearest internal nucleus of the molecule). The frequency of every d_e and d_i combination can be summarised in a 2D fingerprint plot (Figures 6 and S12) which can be broken down by element type for clearer analysis of the intermolecular interactions. The 2D fingerprint plots for all d_e and d_i interactions for **1, 2** and **3** have some similar features due to the shared types of interactions occurring between the complexes in the lattice. In particular, all the complexes share pronounced 'peaks' at low d_e and d_i values, characteristic of hydrogen bonding interactions. To further analyse the 2D fingerprint plot several d_e and d_i combinations of different element types were visualised (figures S13 and S14). Visualisation of the H(internal)···A(external) where A is a suitable hydrogen bond acceptor can be used to analyse hydrogen bonding interactions. For complexes **1** and **3**, the H(internal)···O(external) separations contribute to a similar double-peak pattern in the 2D fingerprint plot, predominantly through the (N)H···O hydrogen bonding interactions of the hydrazide moieties with the perchlorate (**1**) or triflate (**2**) anions (figure S13). However, in **3** which features

fluorine atoms as the hydrogen bond acceptors, there is a more diffuse single peak pattern arising from H(internal)···O(external) separations. Furthermore, a contribution to this diffuse peak pattern is also observed from the H(internal)···N(external) separations due to the presence of an acetonitrile molecule behaving as a hydrogen bond acceptor to a (N)H hydrazide moiety. In comparison, while **1** contains and acetonitrile solvent molecule in the lattice, it does not act as a hydrogen bond acceptor and therefore does not contribute to the peak pattern at low d_e and d_i values. Visualisation of the H(internal)···C(external) and C(internal)···C(external) can be used to compare the (C)H···π and π···π interactions (Figure S14). Complexes **2** and **3** feature similar distributions of H(internal)···C(external) and C(internal)···C(external) separations, commensurate with the similar (C)H···π and π···π interactions occurring in the three structures. In the case of **1**, the distribution of H(internal)···C(external) and C(internal)···C(external) separations is larger which can be rationalised by the presence of benzene molecules in the structure which makes a signification addition to the H(internal)···C(external) and C(internal)···C(external) separations which are otherwise similar to **2** and **3**. Therefore, when quantifying the intermolecular interactions based on the 2D fingerprint plots of larger supramolecular assemblies, care must be taken to consider all molecules in the crystal lattice and not just the complex and counter anions of interest.

Conclusion

In conclusion, were reported the synthesis and structural characterisation of a family of novel dinuclear Co(II) helicates. The variation of the counter anion during the crystallisation had a drastic effect on the crystal packing of the complexes. In particular, despite ClO_4^- and BF_4^- possessing the same tetrahedral geometry, their hydrogen-bonding interactions in complexes **1** and **2** are noticeably different, resulting in significantly different crystal packing. For complexes **1** to **3**, three different forms of π-π interactions of the quinoline ring systems were observed as a result of the different arrangement of the helicate units relative to one another imposed by the differing hydrogen bonding interactions. However, despite these subtlety different interactions, the propensity of the quinoline ring system towards π-π stacking resulted in the formation of two-dimensional supramolecular sheets for all complexes. Analysis of the intermolecular interactions via Hirshfield surface methods provided further insight into the similarities between **1, 2** and **3**. The family of complexes reported in this work are further evidence that quinoline-based ligands are effective supramolecular synthons, in particular when incorporated into metallo-supramolecular species such as dinuclear helicates.

Acknowledgments

Disclosure statement

There are no conflicts to declare.

Funding

ORCID

Benjamin H. Wilson ⓘD http://orcid.org/0000-0003-3739-7489
Paul E. Kruger ⓘD http://orcid.org/0000-0003-4847-6780

References

[1] Albrecht M. "Let's twist again" double-stranded, triple-stranded, and circular helicates. Chem. Rev. **2001**;101 (11):3457–3498.

[2] Piguet C. J Incl Phenom Macrocyclic Chem. **1999**;34 (4):361–391. DOI:10.1023/A:1008079120622.

[3] Piguet C, Bernardinelli G, Hopfgartner G. Helicates as versatile supramolecular complexes. Chem. Rev. **1997**;97(6):2005–2062.

[4] Boiocchi M, Brega V, Ciarrocchi C, et al. Dicopper double-strand helicates held together by additional π–π interactions. Inorg. Chem. **2013**;52(18):10643–10652.

[5] Boiocchi M, Fabbrizzi L. Double-stranded dimetallic helicates: assembling–disassembling driven by the CuI/CuII redox change and the principle of homochiral recognition. Chem Soc Rev. **2014**;43(6):1835–1847.

[6] Fazio E, Haynes CJE, de la Torre G, et al. Chem Commun. **2018**;54(21):2651–2654. DOI:10.1039/C7CC09528G.

[7] Zhao L, Wang J, Wu P, et al. DHPA-containing cobalt-based redox metal-organic cyclohelicates as enzymatic molecular flasks for light-driven H2 production. Sci. Rep. **2017**;7(1):14347.

[8] Martínez-Calvo M, González-Noya AM, Pedrido R, et al. A double-stranded dinuclear cadmium(ii) helicate that assembles into chains in the solid state. Dalton Trans. **2010**;39(5):1191–1194.

[9] Mondal AK, Parmar VS, Biswas S, et al. Tetrahedral MII based binuclear double-stranded helicates: single-ion-magnet and fluorescence behaviour. Dalton Trans. **2016**;45(11):4548–4557.

[10] Pascu GI, Hotze ACG, Sanchez-Cano C, et al. Dinuclear ruthenium(II) triple-stranded helicates: luminescent supramolecular cylinders that bind and coil DNA and exhibit activity against cancer cell lines. Angew. Chem. Int. Ed. **2007**;46(23):4374–4378.

[11] Zou F, Tang X, Huang Y, et al. Fluorescence of a triple-stranded helicate iron(iii) complex from a novel bis-β-diketone ligand: synthesis, structure and spectroscopic studies. CrystEngComm. **2016**;18(35):6624–6631.

[12] Archer RJ, Hawes CS, Jameson GNL, et al. Partial spin crossover behaviour in a dinuclear iron(ii) triple helicate. Dalton Trans. **2011**;40(45):12368–12373.

[13] Archer RJ, Scott HS, Polson MIJ, et al. Varied spin cross-over behaviour in a family of dinuclear Fe(ii) triple helicate complexes. Dalton Trans. **2018**;47 (24):7965–7974.

[14] Pelleteret D, Clerac R, Mathoniere C, et al. Asymmetric spin crossover behaviour and evidence of light-induced excited spin state trapping in a dinuclear iron(ii) helicate. Chem Commun. **2009**;2:221–223. DOI:10.1039/B816196H

[15] Darawsheh M, Barrios LA, Roubeau O, et al. Chem Eur J. **2016**;22(25):8635–8645. DOI:10.1002/chem.201601080.

[16] Estrader M, Salinas Uber J, Barrios LA, et al. A magneto-optical molecular device: interplay of spin crossover, luminescence, photomagnetism, and photochromism. Angew. Chem. Int. Ed. **2017**;56 (49):15622–15627.

[17] Fujita K, Kawamoto R, Tsubouchi R, et al. Spin states of mono- and dinuclear iron(II) complexes with bis-(imidazolylimine) ligands. Chem. Lett. **2007**;36 (10):1284–1285.

[18] Hagiwara H, Tanaka T, Hora S. Synthesis, structure, and spin crossover above room temperature of a mononuclear and related dinuclear double helicate iron(II) complexes. Dalton Trans. **2016**;45 (43):17132–17140.

[19] Li L, Craze AR, Akiyoshi R, et al. Direct monitoring of spin transitions in a dinuclear triple-stranded helicate iron(II) complex through X-ray photoelectron spectroscopy. Dalton Trans. 2018;47(8):2543–2548.

[20] Sunatsuki Y, Kawamoto R, Fujita K, et al. Structures and spin states of bis(tridentate)-type mononuclear and triple helicate dinuclear iron(II) complexes of imidazole-4-carbaldehyde azine. Inorg. Chem. 2009;48 (18):8784–8795.

[21] Tuna F, Lees MR, Clarkson GJ, et al. Readily prepared metallo-supramolecular triple helicates designed to exhibit spin-crossover behaviour. Chem. Eur. J. 2004;10 (22):5737–5750.

[22] Yan Z, Liu W, Peng -Y-Y, et al. Spin-crossover phenomenon in a pentanuclear iron(II) cluster helicate. Inorg. Chem. 2016;55(10):4891–4896.

[23] Golla U, Adhikary A, Mondal AK, et al. Synthesis, structure, magnetic and biological activity studies of bis-hydrazone derived Cu(II) and Co(II) coordination compounds. Dalton Trans. 2016;45(29):11849–11863.

[24] Li H, Chen P, Sun W, et al. Solvent triggered structural diversity of triple-stranded helicates: single molecular magnets. Dalton Trans. 2016;45(7):3175–3181.

[25] Novitchi G, Costes J-P, Tuchagues J-P, et al. A Single Molecule Magnet (SMM) with a helicate structure. New J Chem. 2008;32(2):197–200.

[26] Ayme J-F, Beves JE, Campbell CJ, et al. The self-sorting behavior of circular helicates and molecular knots and links. Angew. Chem. Int. Ed. 2014;53(30):7823–7827.

[27] Ayme JF, Beves JE, Leigh DA, et al. A synthetic molecular pentafoil knot. Nat. Chem. 2012;4:15.

[28] Ayme J-F, Beves JE, Campbell CJ, et al. Template synthesis of molecular knots. Chem Soc Rev. 2013;42(4):1700–1712.

[29] Miyake H, Tsukube H. Coordination chemistry strategies for dynamic helicates: time-programmable chirality switching with labile and inert metal helicates. Chem. Soc. Rev. 2012;41(21):6977–6991.

[30] Malina J, Hannon MJ, Brabec V. DNA binding of dinuclear iron(II) metallosupramolecular cylinders. DNA unwinding and sequence preference. Nucleic Acids Res. 2008;36(11):3630–3638.

[31] Malina J, Hannon MJ, Brabec V. Iron(II) supramolecular helicates interfere with the HIV-1 Tat–TAR RNA interaction critical for viral replication. Sci. Rep. 2016;6:29674.

[32] Meistermann I, Moreno V, Prieto MJ, et al. Intramolecular DNA coiling mediated by metallo-supramolecular cylinders: differential binding of P and M helical enantiomers. Proc Natl Acad Sci. 2002;99(8):5069.

[33] Arunachalam R, Chinnaraja E, Valkonen A, et al. Enantiomeric Resolution of Asymmetric-Carbon-Free Binuclear Double-Stranded Cobalt(III) Helicates and Their Application as Catalysts in Asymmetric Reactions. Inorg. Chem. 2018;57(18):11414–11421.

[34] Chakrabarty R, Mukherjee PS, Stang PJ. Supramolecular coordination: self-assembly of finite two- and three-dimensional ensembles. Chem. Rev. 2011;111 (11):6810–6918.

[35] Desiraju GR. Crystal engineering: from molecule to crystal. J. Am. Chem. Soc. 2013;135(27):9952–9967.

[36] Kruger PE, Martin N, Nieuwenhuyzen M. Dinuclear double helicates with a twist: synthesis, structure and supramolecular entanglement in [M2L2] metallo-helices {M = Co(II),

Cu(II), H2L = bis(N-salicylidene-4,4′-diaminodiphenyl) methane}. Dalton Trans. 2001;13:1966–1970. DOI:10.1039/b102028p

[37] Wilson BH, Scott H, Qazvini OT, et al. A supramolecular porous material comprising Fe(II) mesocates. Chem Commun. 2018;54(54):13391–13394.

[38] Semeniuc RF, Reamer TJ, Smith MD. 8-Quinoline based ligands and their metallic derivatives: a structural and statistical investigation of quinoline π–π stacking interactions. New J. Chem. 2010;34(3):439–452.

[39] Glidewell C, Low JN, Skakle JMS, et al. Hydrogen bonding in nitroaniline analogues: 4-nitrobenzaldehyde hydrazone forms hydrogen-bonded sheets of $R_{\bf 4}^{\bf 4}$(26) rings. Acta Crystallogr Sect C . 2004;60(1):33–34.

[40] Glidewell C, Low JN, Skakle JMS, et al. Hydrogen-bonded dimers in 2-nitrobenzaldehyde hydrazone and a three-dimensional hydrogen-bonded framework in 3-nitrobenzaldehyde hydrazone. Acta Crystallogr Sect C. 2004;60(9):686–689.

[41] Xin P, Zhu P, Su P, et al. Hydrogen-bonded helical hydrazide oligomers and polymer that mimic the ion transport of gramicidin A. J. Am. Chem. Soc. 2014;136 (38):13078–13081.

[42] Zhao X, Wang X-Z, Jiang X-K, et al. Hydrazide-based quadruply hydrogen-bonded heterodimers. Structure, assembling selectivity, and supramolecular substitution. J. Am. Chem. Soc. 2003;125 (49):15128–15139.

[43] Kurbah SD, Kumar A, Sanentiba Ozukum O, et al. Synthesis, characterization, crystal structure, and reactivity of heterobimetallic dioxovanadium(V) complexes containing multidentate hydrazone ligands. J. Coord. Chem. 2017;70(17):2969–2985.

[44] Marchivie M, Guionneau P, Letard J-F, et al. Towards direct correlations between spin-crossover and structural features in iron(II) complexes. Acta Crystallogr Sect B. 2003;59(4):479–486.

[45] Romanović MČ, Milenković MR, Pevec A, et al. Crystal structures, magnetic properties and DFT study of cobalt-(II) azido complexes with the condensation product of 2-quinolinecarboxaldehyde and Girard's T reagent. Polyhedron. 2018;139:142–147.

[46] Mori A, Suzuki T, Nakatani Y, et al. Dalton Trans. 2015;44 (36):15757–15760. DOI:10.1039/C5DT02345A.

[47] Qi B, Guo X, Gao Y, et al. Strong co-ion effect via cation −π interaction on the self-assembly of metal–organic cationic macrocycles. J. Am. Chem. Soc. 2017;139 (34):12020–12026.

[48] Wu D-F, Shen H-Y, Chu X-Y, et al. New J Chem. 2018;42 (20):16836–16845. DOI:10.1039/C8NJ02888E.

[49] McKinnon JJ, Jayatilaka D, Spackman MA. Towards quantitative analysis of intermolecular interactions with Hirschfeld surfaces. Chem Commun. 2007;37:3814–3816. DOI:10.1039/b704980c

[50] Spackman MA, Jayatilaka D. Hirshfeld surface analysis. CrystEngComm. 2009;11(1):19–32.

[51] Spackman MA, McKinnon JJ. Fingerprinting intermolecular interactions in molecular crystals. CrystEngComm. 2002;4(66):378–392.

[52] Wolff SK, Grimwood DJ, McKinnon JJ, et al. CrystalExplorer (Version 3.1). University of Western Australia; 2012.